Intramolecular hydrogen bonding in articaine can be related to superior bone tissue penetration: A molecular dynamics study

Åge Aleksander Skjevik [a], Bengt Erik Haug [b,c], Henning Lygre [d], Knut Teigen [a,*]

[a] Department of Biomedicine, University of Bergen, N-5009 Bergen, Norway
[b] Department of Chemistry, University of Bergen, Allégaten 41, N-5007 Bergen, Norway
[c] Centre for Pharmacy, Department of Chemistry, University of Bergen, N-5007 Bergen, Norway
[d] Section of Pharmacology, Institute of Medicine, University of Bergen, N-5020 Bergen, Norway

ABSTRACT

Local anesthetics (LAs) are drugs that cause reversible loss of nociception during surgical procedures. Articaine is a commonly used LA in dentistry that has proven to be exceptionally effective in penetrating bone tissue and induce anesthesia on posterior teeth in maxilla and mandibula. In the present study, our aim was to gain a deeper understanding of the penetration of articaine through biological membranes by studying the interactions of articaine with a phospholipid membrane. Our approach involves Langmuir monolayer experiments combined with molecular dynamics simulations. Membrane permeability of LAs can be modulated by pH due to a titratable amine group with a pKa value close to physiological pH. A change in protonation state is thus known to act as a lipophilicity switch in LAs. Our study shows that articaine has an additional unique lipophilicity switch in its ability to form an intramolecular hydrogen bond. We suggest this intramolecular hydrogen bond as a novel and additional solvent-dependent mechanism for modulation of lipophilicity of articaine which may enhance its diffusion through membranes and connective tissue.

1. Introduction

Articaine is a small molecule drug commonly used as a local anesthetic by dentists to alleviate pain during dental procedures. It is one of many local anesthetics (LAs), a collection of drugs sharing some structural characteristics in that they contain a hydrophobic aromatic part and a basic secondary or tertiary amine [1]. In the two major classes of local anesthetics the hydrophobic part and the amine are linked either through an ester or amide bond, giving rise to amino ester or amino amide local anesthetics. Articaine belongs to the latter group, and the structures of articaine and lidocaine, the most commonly used drugs from this group, are shown in Fig. 1.

Although articaine contains the same basic structural characteristics as the other amino amide local anesthetics, it has some unique features. As opposed to most of the other amino amide LAs, it has a thiophene ring as the aromatic moiety. Furthermore, it contains an aromatic methoxycarbonyl substituent, a structural element not present in the other members of this group. Both features are pharmacokinetically advantageous. The methoxycarbonyl substituent makes articaine a suitable substrate for plasma cholinesterases, the consequence being a short half-life. The presence of the methoxy-carbonyl-substituted thiophene is generally accepted to contribute to a higher lipophilicity of articaine compared to the other amino amide local anesthetics [2], and articaine shows a better ability to penetrate bone and tissue compared to LAs in general [3,4]. Articaine has provided a higher success rate than lidocaine in anesthetizing mandibular and maxillary posterior teeth by buccal infiltration [5–7], and the prescence of the thiophene ring has been suggested as a plausible explanation [6]. As a supplement to lidocaine inferior alveolar nerve block (IANB), articaine buccal infiltration also produced a higher degree of pulpal anesthesia of mandibular teeth than was the case with IANB alone [8]. Lidocaine, on the other hand, did not significantly increase the efficacy of lidocaine IANB in an analogous experiment [9]. Articaine's favourable diffusion properties has inspired studies where it is utilized clinically. It has for instance been successfully added to a local anesthetic regimen originally containing lidocaine and bupivacaine for surgery taking place close to the muscular fascia [10]. The authors report previous difficulties in anesthetizing this area satisfactorily with other amide LAs, and that required consistent pain relief is achieved with articaine as an adjunct. In addition, limited diffusion of LAs has been the main argument for
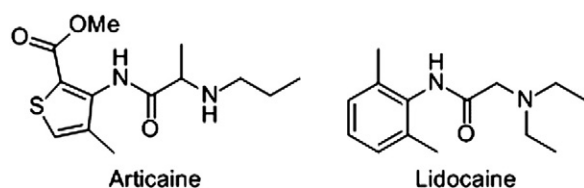
Fig. 1. Two amino amide local anesthetics, articaine and lidocaine.

trying articaine as a peribulbar anesthetic in cataract surgery, where it has proved to be more efficient than the mixture of lidocaine and bupivacaine conventionally injected [11].

Despite the clinical discoveries, the exact molecular mechanism of articaine action is not apparent. LAs are known to inhibit the passage of electrical signals in certain nerve fibers [1]. They thereby prevent impulses usually interpreted as pain from reaching their destination in the brain. The most widely accepted theory of the mechanism involves crossing of the LA through the neuronal membrane, followed by specific inhibition of transmembrane sodium channels responsible for the initiation and transport of signals along the nerve cell [1]. Access to the binding site is proposed to be from the axoplasmic side. Articaine is no exception and appears to exert its local anesthetic effect by the same mechanism [12]. The structural characteristics common to all LAs are of the utmost importance to the mechanism of action and their function as pain relieving remedies. In order to be efficient and potent, the LA has to be hydrophilic enough to stay in solution, yet sufficiently hydrophobic to permeate nerve sheath. The pKa values for the secondary and tertiary amines of the local anesthetics are in the range of 7.6–8.2, except for dibucaine which is the strongest base with a pKa of 8.8. Articaine has a pKa value of 7.8 [13]. Consequently, about 28.5% of the molecules will be neutral at physiological tissue pH, ensuring that a sufficient proportion of the drug is readily available for diffusion into the axoplasm and able to reach the site of action. In addition to the well-established receptor-mediated mechanism of action for local anesthetics, biological membranes have been suggested as the primary target (for a review, see [14]). Similar non-specific non-receptor mediated modes of action have been postulated for other drugs currently in clinical use, e.g. for the antipsychotic drugs chlorpromazine [15] and olanzapine [16]. These drugs are thought to indirectly influence function of membrane proteins by altering membrane properties through intercalation into the lipid bilayer. Interestingly, lidocaine has been found to increase the electrostatic potential of a membrane, as investigated by molecular dynamics (MD) simulations [17]. The changes were concluded to be significant enough to potentially interfere with the normal function of sodium ion channels spanning the membrane.

Even though articaine is an approved drug, it seems that much remains to be elucidated regarding the mechanisms by which it exerts its pharmacological effects. Such detailed knowledge is of importance in the era of rational, structure-based drug design, and we believe that computational methodology has the potential of contributing to a deeper understanding in this respect. Molecular dynamics (MD) simulations is a deterministic method capable of predicting time-resolved atomic scale dynamics of a system. As such, it is valuable for investigating molecular mechanisms. Performing and developing methods for MD simulations on biological membranes is challenging. Because of the inherent fluidity of lipid bilayers, there is not a great deal of experimental data of high detail to validate simulations [18]. The challenge faced is reflected in difficulties in reproducing experimental findings in membrane simulations. One such difficulty is to reproduce the area per lipid without either adding surface tension [19–23] or using constant volume [24–26] or fixed cross-sectional area [27–31]. Nevertheless, experimentally validated areas per lipid have recently been achieved in tensionless constant pressure simulations of phosphatidylcholine bilayers with CHARMM [32–34] and GROMOS [35] force fields.

The aim of the present study was to gain insight into how articaine interacts with biological membranes by applying the experimental Langmuir monolayer technique in combination with all-atom MD simulations within the AMBER program package [36,37]. As a membrane model for MD simulations we have used a bilayer composed solely of 1-palmitoyl-2-oleoyl-sn-glycero-3-phosphocho-line (POPC, see Fig. 2), and equilibration and validation of the membrane were prerequisites for obtaining reliable results.

The Langmuir monolayer technique was employed to establish intercalation of articaine into POPC monolayers and to determine the area occupied by each lipid, an important experimental quantity in validation of lipid membrane simulations. There are no specific lipid parameters within AMBER. However, the general amber force field (GAFF) [38] has been applied for simulations of phospholipid membranes [21,22,39], and we also decided to use GAFF.

2. Materials and methods

2.1. Langmuir monolayer experiments

1-palmitoyl-2-oleoyl-sn-glycero-3-phosphocholine (POPC) was supplied in powder form by Avanti Polar Lipids Inc. $Na_2HPO_4 \cdot 12 H_2O$ and $NaH_2PO_4 \cdot H_2O$ were obtained from Fluka Chemika and Merck, respectively. The subphase buffer (10 mM $Na_2HPO_4 \cdot 12 H_2O$, 10 mM $NaH_2PO_4 \cdot H_2O$, pH 7.0) was prepared in Milli-Q water. POPC was dissolved in chloroform to give a 1 mg/mL lipid solution. Langmuir compression experiments [40] were performed using a KSV Minitrough made of Teflon with two movable, symmetric Delrin barriers (KSV Instruments Ltd, Helsinki, Finland). Subphase buffer temperature was kept constant at 27 ± 1 °C in all experiments by a thermostat connected to the trough. The surface of the subphase was cleaned with a Pasteur pipet linked to a vacuum pump in order to remove any dust particles present before addition of the lipid monolayer. 20 μL of lipid solution was applied cautiously to various sites on the surface of the subphase, drop by drop using a Hamilton syringe. Chloroform was allowed to evaporate for an interval of at least 5 min between application and start of the compression. Barriers were compressed with a constant rate of 5 mm/min. A platinum Wilhelmy plate, in combination with an electric balance, recorded the changes in surface pressure, giving rise to surface pressure-area isotherms. Three parallels were carried out.

Articaine hydrochloride powder from Denamed AS (Strømmen, Norway) was dissolved in the buffer to give a 25 mg/mL articaine solution. Thereafter, an L-shaped syringe was used to inject the LA into the subphase of a POPC monolayer film already compressed to 30 mN/m, as described by Glomm et al. [41]. Care was taken not to influence or disrupt the monolayer. In order to optimize drug uniformity in the subphase, the syringe was moved from side to side along the bottom of the trough while 2 mL of articaine solution were injected slowly and carefully, resulting in a final articaine concentration of about 200 μg/mL in the subphase buffer. Half of the drug solution was injected from the outside of one barrier and the other half from outside of the other barrier. Air bubbles were removed from the syringe prior to the injection procedure. The mean molecular area recorded as a function of time and at the constant surface pressure of 30 mN/m was a qualitative measurement of articaine intercalation.
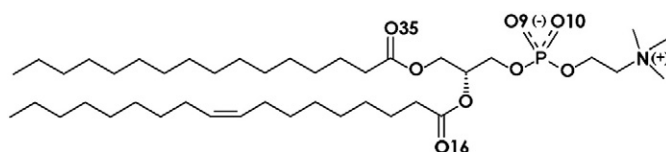

Fig. 2. POPC structure. Schematic representation of palmitoyl-oleoyl-phosphatidylcho-line with atom names (O#) denoting oxygens referred to in the text.

2.2. MD simulations

Electrostatic potential surfaces were calculated at the HF/6-31G* level with Gaussian03 [42] and atomic point charges fitted by a RESP procedure [43]. GAFF atom types [38] were assigned with Antechamber [44]. GAFF has previously been applied to simulate lipid membranes with constant surface tension [21,22]. The starting point for generation of atomic point charges for POPC was the PDB of a membrane from the Karttunen Group website, Department of Applied Mathematics, University of Western Ontario [45]. Previously simulated for 30 ns and consisting of 128 POPC molecules, this bilayer contained a representative collection of conformations. As a compromise between computational efficiency and structural diversity, six conformationally divergent POPC lipids were chosen to constitute the basis for charge derivation for our all-atom model. The average point charges calculated for the whole lipid molecule from these six conformations were used in POPC simulations.

All the minimizations and simulations were performed with the AMBER 9 program package [37]. GAFF parameters and self-developed charges were used for lipids and articaine (Fig. 3), while water molecules were of the TIP3P model [46].

The systems were placed in periodic boxes, and electrostatic interactions summed by the particle mesh Ewald method [47,48] using a fourth-order B-spline interpolation, a grid spacing below 1 Å and a direct sum tolerance of 10^{-5}. To truncate van der Waals forces, a cut-off of 10 Å was applied. The SHAKE algorithm [49] was used to constrain covalent bonds involving hydrogen atoms, allowing for a time step of 2 fs. Anisotropic pressure scaling was applied during constant pressure simulations, with a target of 1 bar in each dimension. Initial simulations under these conditions, without positional restraints, produced membranes that were too highly compressed (data not shown), as observed for similar systems in the literature [21,22,34,35,50]. Commonly employed approaches to circumvent this problem have been application of a constant positive

surface tension to increase the lateral area of the membrane [19–23] or to keep the cross-sectional area of the bilayer fixed [27–31]. However, these functionalities are not currently implemented in Amber and we followed an alternative approach to restrain the cross sectional area of our membrane. Positional restraints were applied to the lipids lining the simulation box in order to conserve area per lipid during density adjustment before constant volume was used for production runs. The *NVT* ensemble has previously been applied to successfully simulate lipid membranes with Amber [26]. In addition, Prates et al. [51] applied a similar setup to simulate articaine in presence of a POPC lipid bilayer. In this study articaine was simulated with parameters for the CHARMM c35b2 release of the force field [52] with the NAMD simulation engine [53], applying constant surface area corresponding to an area per lipid of 65 $Å^2$. During heating and equilibration, the Langevin thermostat [54] regulated the temperature. On changing to production runs, it was replaced by the Berendsen thermostat [55]. Simulation temperature was kept at 300 K, well above the phase transition temperature of −2 °C for POPC [56]. Different force constants for positional restraints were applied; 500 kcal/mol $Å^2$ for minimization and 10 kcal/mol $Å^2$ for equilibration simulations. Snapshots from every 10th ps of the simulations were saved and used for processing in AMBER ptraj and for visualization of the dynamics in VMD [57].

The initial configuration of the pure POPC membrane was the previously mentioned PDB from the Karttunen Group website [45], consisting of 128 POPC molecules in a bilayer hydrated by 3655 water molecules and with an area per lipid of 64.8 $Å^2$. Minimization and equilibration of the pure bilayer was carried out as follows: (i) Minimization for 2000 steps with positional restraints on heavy atoms (non-H atoms) of the lipids; (ii) Minimization for 5000 steps without restraints; (iii) 50 ps heating from 0–300 K with *NVT* ensemble (constant number of particles (N), volume (V) and temperature (T)) and positional restraints on the lipids; (iv) 5 ns equilibration with *NPT* (constant number of particles (N), pressure (P) and temperature (T))
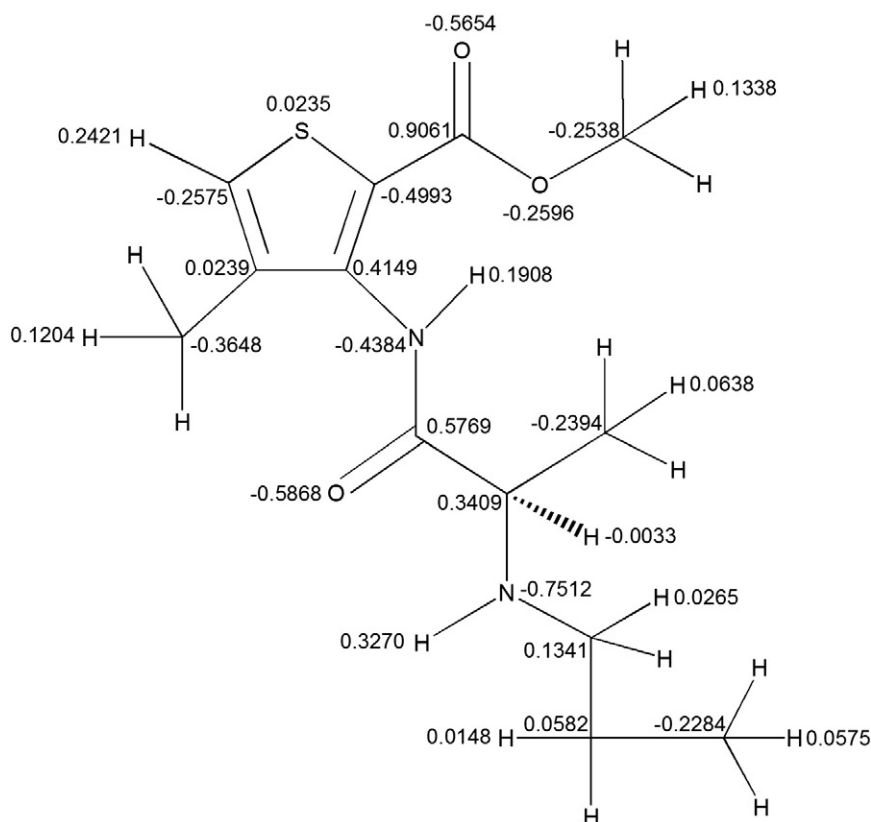

Fig. 3. The structure of neutral (*R*)-articaine and derived atomic point charges.

ensemble, anisotropic pressure scaling at 1 atm and positional restraints on the lipids lining the box edges; (v) 60 ns simulation at constant pressure (*NPT*) without positional restraints. This procedure was found to produce unrealistic behavior of the bilayer and we therefore switched to simulate at constant volume also for (v) above. See further elaboration on this under the results section. Starting conformation of the lipid bilayer together with neutral (*R*)-articaine (denoted (*R*)-A) and positively charged (*R*)-articaine (denoted (*R*)-AH⁺) was based on the equilibrated bilayer after 60 ns of *NVT* simulation. Initial coordinates for the articaine-POPC system was prepared by molecular docking with the Dock 6.1 software [58]. The leaflet defined as "receptor" for docking was extracted from the end structure of the pure lipid bilayer simulation. Water was removed from the coordinates prior to receptor preparation and the highest ranked conformation of(*R*)-A and (*R*)-AH⁺, evaluated by a force field based scoring function [59], was selected for MD simulations. Water molecules present in the original lipid bilayer were reintroduced and solvent residing within 1 Å of the articaine molecule was deleted. Generation of periodic boxes and subsequent topology and coordinate files resulted in two different simulation systems (A and B in Table 1). An additional model (system C) for neutral (*S*)-articaine was created from the system containing neutral (*R*)-articaine. Charges were derived and GAFF atom types assigned by the use of Gaussian [42], RESP [43] and Antechamber [44]. Each articaine-POPC system (systems A–C in Table 1) contained one articaine molecule.

The same protocol as applied for equilibrating the lipid bilayer (as previously discussed) was used for the membrane–articaine complexes (systems A–C in Table 1), except that the final *NVT* run was increased from 60 ns to 100 ns to produce trajectories for analysis. In addition, simulations of neutral articaine species in water (systems D and E in Table 1) were conducted, for which the procedure was as follows: i) Minimization for 1000 steps; ii) 100 ps equilibration at 300 K with *NPT* ensemble; iii) 500 ns simulation with *NPT* ensemble. Starting conformations of articaine were the same as for the POPC simulations.

Trajectory analyses were mainly done with AMBER ptraj. The degree of order in the acyl chains of membrane lipids can be quantified by means of deuterium order parameters (S_{CD}). High S_{CD} values signify a high degree of order and vice versa. Order parameters for the palmitoyl (sn-1) and oleoyl (sn-2) acyl chains were calculated from the last 16 ns of the *NPT* and *NVT* simulations of the pure POPC membrane using the following equation:

$$S_{CD} = 0.5\langle 3cos^2\theta - 1\rangle \qquad (1)$$

θ is the angle between the bilayer normal and the C–H vector for a given carbon atom in the hydrocarbon tail. Z translation analysis was performed with the g_traj application included in GROMACS 4.0.5 [60]. g_traj extracted the z coordinates for the center of mass (CM) of the monolayer phosphorus atoms and the corresponding coordinates for the CM of articaine from each trajectory. The distance in the z dimension between the centers of mass of the phosphorus atoms in each leaflet was treated as POPC membrane thickness. The hydrogen

bonding facility of ptraj (hbond) was utilized to quantify interactions in the simulations. For an interaction to be regarded as a hydrogen bond, the distance between the non-hydrogen atoms had to be less than 3.5 Å and the donor-hydrogen-acceptor angle greater than 120°. Hbond returns only details about individual bonds. As an additional analysis, we used only the distance (3.5 Å) as criterion for hydrogen bonds, as this made it possible to group similar and simultaneously present interactions as one single hydrogen bond occurrence (see Results section).

3. Results

3.1. Langmuir monolayer experiments

The Langmuir compression experiments performed on monolayers of POPC resulted in an area per lipid of 64.0 ± 0.3 Å² at 30 mN/m. Results from three parallel runs are presented in Fig. 4.

In the articaine injection experiments the POPC monolayer was allowed to equilibrate for a couple of minutes at 30 mN/m before articaine was injected into the subphase. The choice of surface pressure originated from the proposed internal lateral pressure of biological membranes, suggested to be 30–35 mN/m [61]. The presence of articaine caused the barriers to move and induced a 12–13% increase in the mean molecular area of the monolayer film in two parallels.

3.2. Molecular dynamics simulations

Membrane thickness for the constant pressure simulation equilibrated after about 40 ns and remained stable at 44.30 ± 0.28 Å over the last 20 ns of pure POPC simulation. The thickness of the bilayer remained stable at 38.43 ± 0.14 Å for the entire constant volume simulation, and the area per lipid was 64.3 Å². Order parameters (S_{CD}) for the sn-1 palmitoyl and sn-2 oleoyl acyl chains were calculated over the last 16 ns of both pure POPC simulations. The computed values from the two simulations are shown in Fig. 5, along with experimental data derived from deuterium NMR spectroscopy [62,63].

The initial constant pressure simulation of the POPC bilayer produced unrealistic behavior with respect to area occupied per lipid, membrane thickness and order parameters. The membrane simulated with constant volume was found to better reproduce experimentally observed values for thickness and deuterium order parameters. Simulations with (*R*)-AH⁺ in complex with the POPC membrane resulted in trajectories where the articaine molecule made stable electrostatic interactions with the lipid headgroups throughout
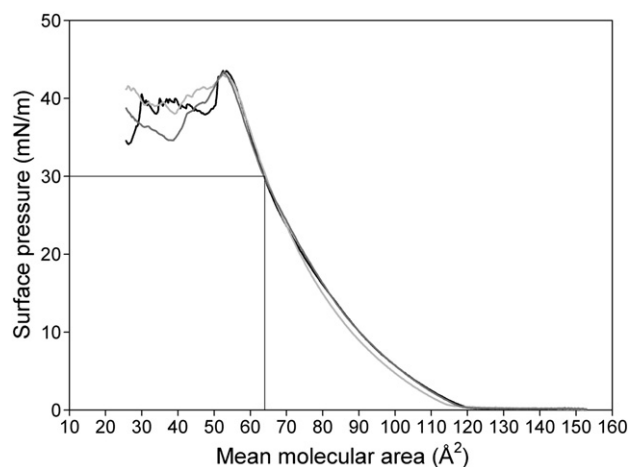
Table 1
Summary of the different articaine simulation systems in the present study.

System	Articaine form[a,b]	Number of POPC	Number of TIP3P waters	Simulation time[c]
A	(*R*)-A	128	3644	100 ns
B	(*R*)-AH⁺	128	3645	100 ns
C	(*S*)-A	128	3644	100 ns
D	(*R*)-A	–	859	500 ns
E	(*S*)-A	–	886	500 ns

[a] (*R*) and (*S*) denote the R and S enantiomer, respectively.
[b] AH⁺ = positively charged; A = neutral.
[c] Heating step excluded.

Fig. 4. Langmuir compression isotherms. The three parallels for POPC are represented by black, dark gray and light gray lines. The NaH₂PO₄/Na₂HPO₄ subphase buffer of pH 7 was kept at 27 ± 1 °C. At 30 mN/m the area per lipid was found to be 64.0 ± 0.3 Å².
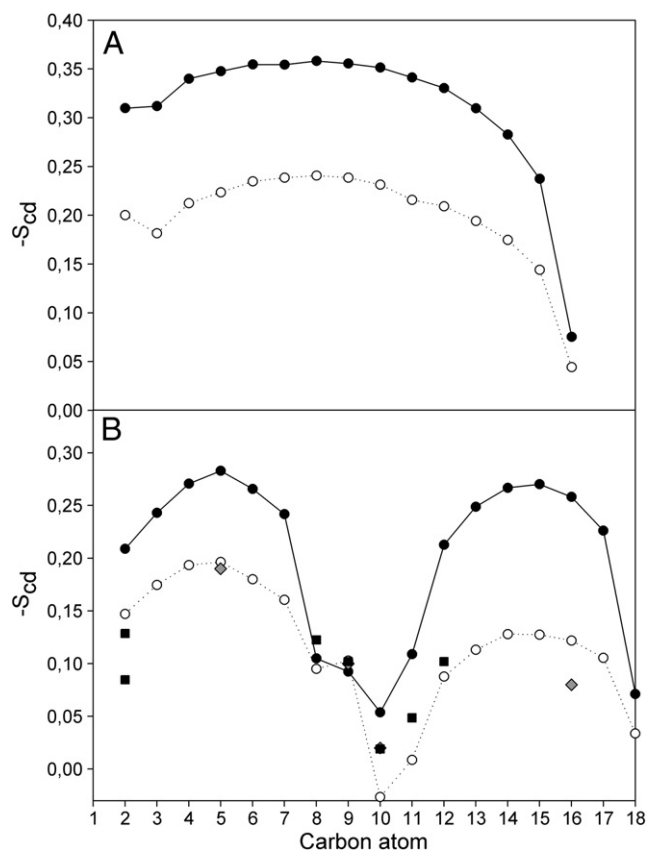
Fig. 5. Deuterium order parameters for the sn-1 palmitoyl (Panel A) and sn-2 oleoyl (Panel B) chains computed from the last 16 ns of the NPT (black solid line with filled circles) and the NVT (dotted line with open circles) simulations of the pure POPC bilayer system. The black squares and the dark gray diamonds represent experimental data recorded at 27 °C [63] and 30 °C [62], respectively.

the simulation, preventing complete intercalation into the membrane interior. The neutral forms of articaine, (R)-A and (S)-A, did not make strong interactions with the headgroups and were observed to penetrate into the membrane interior. The trajectories were subjected to various analyses and Fig. 6 shows the translation of articaine (center of mass) along the bilayer normal (Z translation).

The bar charts in Fig. 7 depict important hydrogen bond occurences, both within articaine and between articaine and POPC
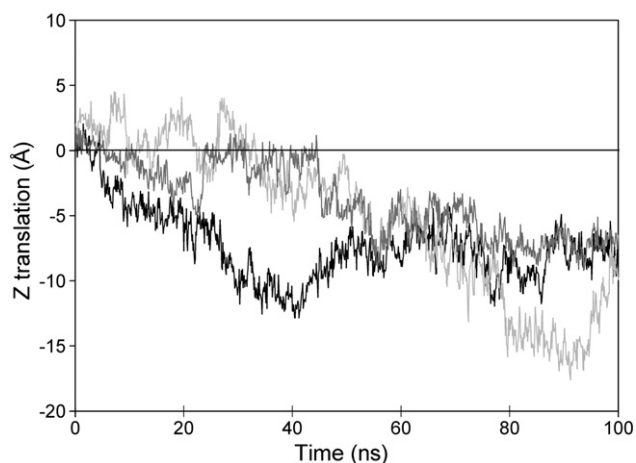

Fig. 6. Z translation analyses. Movement along the bilayer normal for the center of mass of neutral (R)-articaine (black line), positively charged (R)-articaine (dark gray line) and neutral (S)-articaine (light gray line) in the POPC membrane system. Zero on the y axis denotes the center of mass of the phosphorus atoms in the membrane leaflet.
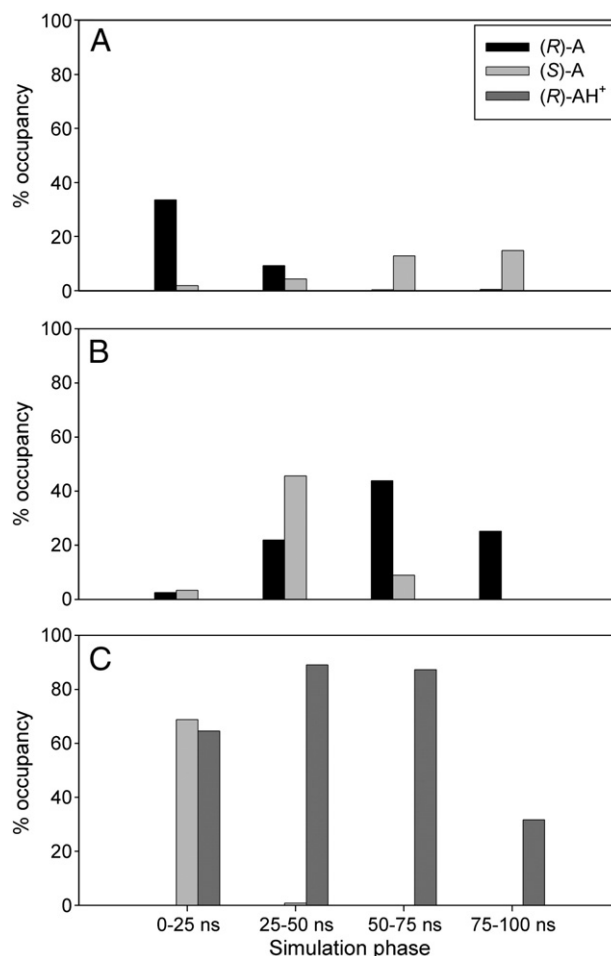

Fig. 7. Hydrogen bond distance analysis. Each of the panels show the occupancies of different hydrogen bond occurrences taking place either within articaine or between the LA and POPC lipids in systems A to C in Table 1. Panel A: The internal hydrogen bond between the amine nitrogen and the ester carbonyl oxygen (for illustrative snapshots, see Fig. 8). Panel B: Hydrogen bond interaction between the LA and fatty acid carbonyl oxygens in POPC (atoms O16 and O35 in Fig. 2). Panel C: Hydrogen bond occurrence between articaine and phosphate oxygens in POPC (atoms O9 and O10 in Fig. 2). Simulation time has been divided into four equally spaced intervals, resulting in four sequential phases on the x axis, each comprising 25 ns. Neutral (R)-articaine is represented by black bars, neutral (S)-articaine by grey bars and positively charged (R)-articaine by brown bars in all three panels.

lipids (O9/O10 and O16/O35 in Fig. 2). Simulation time has been divided into four sequential phases, each consisting of 25 ns, to describe the intercalation event. An intramolecular hydrogen bond between the carbonyl oxygen of the methoxycarbonyl substituent and the secondary amine (see Figs. 1 and 7) was formed in both (R)-A and (S)-A. A similar intramolecular hydrogen bond was not observed for (R)-AH$^+$.

This internal hydrogen bond occurrence is correlated with the entrance of articaine into the membrane interior, as illustrated in Fig. 8, which shows the first 10 ns of the (R)-A/POPC simulation with concurrent breaks in all three curves between the 4th and 5th nanoseconds.

Simulations of (R)-A and (S)-A in aqueous surroundings (systems D and E in Table 1) were conducted for the sake of comparison with the behavior of the same molecules interacting with the POPC membrane, focusing on the possible formation of the internal hydrogen bond previously mentioned. The intramolecular hydrogen bond existed 0.2% of the time when (R)-A explored conformational space in pure water compared to 8.1% in the membrane simulation. The corresponding occupancies derived for (S)-A in water and in the membrane system were 0.8% and 4.6%, respectively.
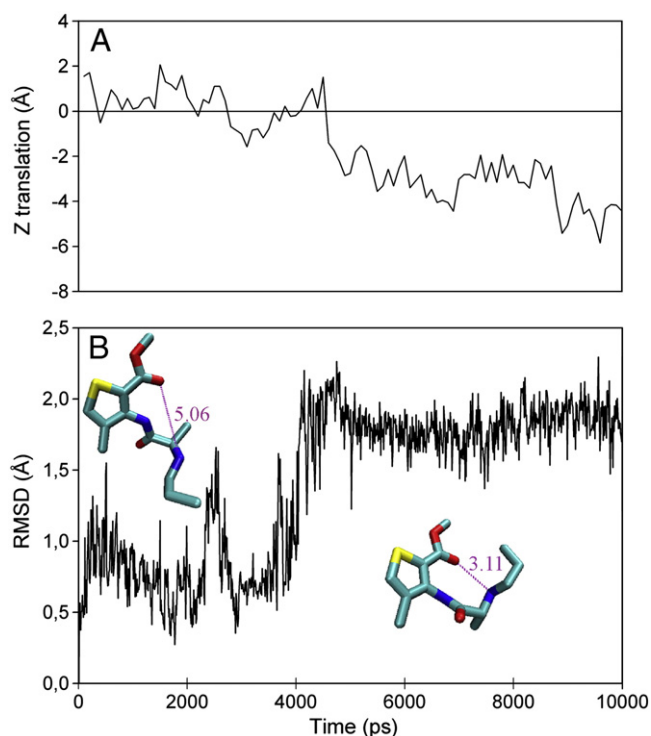
Fig. 8. Trajectory analyses from the first 10 ns of the simulation of neutral (R)-articaine and POPC as functions of simulation time. Panel A: Z translation for the center of mass of articaine. Panel B: RMSd of articaine. The starting structure was used as the reference. The snapshots shown are representative of the conformations seen before (left) and after (right) the RMSd transition occurring between the fourth and fifth nanosecond. To avoid noise, hydrogens are not shown. The dashed purple line and the accompanying purple number represent the intramolecular distance (Å) between the amine nitrogen and the ester carbonyl oxygen.

4. Discussion

Our experimentally determined area per lipid of 64.0 ± 0.3 Å^2 for POPC (Fig. 4) is close to a previously reported area per lipid of 63 Å^2, also found by Langmuir compression of a POPC monolayer [64]. In this previous study the buffer subphase had a pH of 6.6 and the temperature was set to 24 ± 1 °C, which may account for the slight discrepancy between the obtained areas per lipid. However, several different examples of experimental areas appear in the literature, where different methods and conditions have been applied [65–67]. In conclusion, an area of 64.3 Å^2 per lipid for our MD simulations seems reasonable in relation to our Langmuir experiments as well as other experimental studies. The injection method [41] enabled us to adjust the surface pressure of the POPC monolayer to the physiological value of 30 mN/m prior to injecting articaine. The observed 12–13% increase in mean molecular area can be ascribed to intercalation of articaine into the monolayer.

The experimental membrane thickness of a POPC bilayer, defined as the separation between electron density maxima obtained from X-ray scattering experiments, has been found to be 37 Å at 30 °C [66]. The average membrane thickness calculated from our constant volume simulation, defined as the distance between the center of mass of phosphorous atoms in the two leaflets, was found to be 38.43 ± 0.14 Å and is in fairly good agreement with experiment. Deuterium order parameters for the oleoyl acyl chain calculated from our NVT simulation are in good agreement with S_{CD} parameters obtained by NMR for POPC [62,63]. Corresponding values for the palmitoyl acyl chain also agree fairly well with experimental data [68], indicating that our NVT simulations are able to reproduce experimentally observed behavior. For both acyl chains, order parameters from the NVT simulation lie

significantly closer to NMR data than the ones obtained with the NPT ensemble.

From Fig. 6 it appears that (R)-AH$^+$ and the neutral forms intercalate almost equally well into the hydrophobic core of the lipid bilayer. This plot shows the center of mass of the articaine molecules with respect to the bilayer normal. However, the orientations of the articaine molecules are different with (R)-AH$^+$ accomodating a snorkeling orientation and remaining at the interfacial region with only the thiophene ring buried into the hydrophobic part of the membrane. The neutral forms, on the other hand, were totally embedded in the lipophilic environment, in a less extended conformation. The difference in preferential locations is also evident from what interactions the different articaine molecules participated in (Fig. 7). (R)-AH$^+$ was found to interact extensively with POPC phosphate oxygen atoms throughout the simulation (Panel C), in agreement with consistent snorkeling behavior which is a mechanism thought to be involved in the interaction of peptides and proteins with membranes [69].

Both enantiomers of the neutral state of articaine intercalated into the POPC membrane in the MD simulations. Articaine intercalation and incorporation into membranes have also been indicated experimentally, both in this work and by others [70,71]. The general observations of snorkeling and differences in penetration depth are reminiscent of findings in a MD simulation study of charged and neutral lidocaine molecules in a DMPC bilayer [72]. The study is of relevance, considering both the structural similarities between articaine and lidocaine and the use of a phosphatidylcholine membrane model. Interestingly, lidocaine altered the electrostatic potential of the DMPC membrane to such a degree that it was suggested to influence the function of ion channels in the membrane [17].

The most striking observation in this study was the formation of an intramolecular hydrogen bond and its implication for the intercalation of neutral articaine into the hydrophobic interior of the lipid membrane. It is evident from Fig. 6 that (R)-A quickly descends from the membrane/water interface and into the hydrophobic region of the POPC bilayer. The decisive event is the formation of the internal hydrogen bond, as shown in Fig. 8 that focuses on the first 10 ns of simulation. Panel A shows translation of articaine along the bilayer normal, indicating that articaine enters the membrane interior after 4 ns of simulation. Panel B shows the interatomic distance between the secondary amine nitrogen and the carbonyl oxygen of the methoxycarbonyl substituent in (R)-A indicating that a stable hydrogen bond is formed at the same time as articaine enters the membrane. Representative conformations of the "pre" and "post" hydrogen bond ensembles are shown in the plot. Thus, it seems apparent that the ability to form an intramolecular hydrogen bond has an effect on the lipophilicity of articaine, as has been shown for other compounds [73], and is the decisive event for intercalation into the POPC bilayer in our simulations. This intramolecular hydrogen bond was also observed for (S)-A with a calculated occupancy of 4.6% in the membrane simulation (versus 0.8% in water). Even so, bond formation was hampered in the first phase of the simulation by a favorable interaction between the amide in articaine and a POPC phosphate oxygen (Panel C in Fig. 7). Breakage of this interaction was immediately followed by diffusion of (S)-A into the membrane. The general behavior and interactions of (R)- and (S)-articaine with the membrane are similar and the observed minor differences are most probably related to the simulations exploring phase space somewhat differently.

Substantially higher occupancies of the intramolecular hydrogen bond in (R)-A and (S)-A were observed in the articaine-membrane simulations than in the articaine-water simulations (systems D and E in Table 1). It was practically not present in aqueous surroundings, the very low occupancies being almost negligible. Still, in contact with the POPC membrane, either at the interface or inside, the hydrogen bond was considerably more stable. Hence, the molecule's tendency for the internal bond formation seems to be strongly dependent on the surrounding environment. This behavior of articaine is similar to what

has been found in simulations performed with parameters developed for the CHARMM force field [51]. The authors describe a difference in conformational space explored by articaine that is dependent on the environment. In aqueous environment articaine is able to form hydrogen bonds with water molecules while it is more compact and has a lower dipole moment in the POPC bilayer. Although the authors do not explicitly describe an internal hydrogen bond, it appears that their compact "U-shaped" articaine conformation observed in the POPC membrane is very similar to our conformation (Fig. 7B). Our results correlate very well with those of Prates et al. [51], indicating a conformational preference of articaine that is dependent on the environment. In hydrophobic surroundings the drug is able to form an internal hydrogen bond, which reduces its conformational flexibility, dipole moment [51] and hydrophilicity.

The better ability of articaine to traverse bone and tissue compared to the other LAs has been ascribed to the thiophene ring [4,6,3]. However, *thiophene itself is actually less hydrophobic than benzene*, and the experimentally measured logP values for the two compounds are reported to be 1.81 and 2.13, respectively [74]. Substituted thiophenes are also consistently reported to have lower experimentally determined logP values than the corresponding substituted benzene derivatives [74]. On the other hand, it may very well be that it is instead the *intramolecular hydrogen bond* that contributes to give articaine its favorable properties. The contribution of intramolecular hydrogen bonds to increased lipophilicity of small molecules has recently been clearly demonstrated [73]. It was consistently found that derivatives devoid of the ability of intramolecular hydrogen bond formation were less lipophilic based on experimentally measured logD values. In the same study it was found that calculated logP (clogP) values for small molecules capable of forming intramolecular hydrogen bonds were underestimated by a value of 0.4 for each bond [73]. By virtue of intra- or intermolecular hydrogen bonds, the polar surface area of both small organic molecules and natural products are postulated to enhance lipid solubility and thereby membrane permeability [73,75]. As such, the observed intramolecular hydrogen bond in our simulations can be implicated in the success of articaine in certain clinical situations where other LAs have been less effective or inadequate [5,6,8,10,11]. Accordingly, our simulations imply that the methoxycarbonyl substituent has functional implications beyond making articaine a suitable substrate for cholinesterases which leads to rapid inactivation. As pointed out before, the methoxycarbonyl substituent is not found in other amino amide LAs [76].

5. Conclusion

In conclusion, we propose that the lipophilicity of articaine can be modulated by the formation of an intramolecular hydrogen bond in addition to the general pKa-dependent switch between protonation states used by all LAs. The potential for internal hydrogen bonds is thus an important aspect to consider in the design of new LAs and other drugs that should be able to cross hydrophobic barriers, without diminishing solubility in water. The ability of articaine to form an internal hydrogen bond, as observed in our MD simulations, appears to be a mechanism unique to articaine, enabling an increased lipid solubility, which may explain its superior bone and tissue penetration and anesthetic efficacy on posterior maxillary and mandibular teeth, compared to other LAs.

Acknowledgments

References

[1] D.E. Becker, K.L. Reed, Essentials of local anesthetic pharmacology, Anesth. Prog. 53 (2006) 98–109.
[2] T. Lemke, D. Williams, V. Roche, S. Zito, Foye's Principles of Medicinal Chemistry, 6th Edition (Wolters Kluwer, Lippincott Williams & Wilkins, 2008).
[3] S. Malamed, What's new in local anaesthesia? SAAD Dig. 25 (2009) 4–14.
[4] T.B. Vree, M.J.M. Gielen, Clinical pharmacology and the use of articaine for local and regional anaesthesia, Best Pract. Res. Clin. Anaesthesiol. 19 (2005) 293–308.
[5] M.D. Kanaa, J.M. Whitworth, I.P. Corbett, J.G. Meechan, Articaine and lidocaine mandibular buccal infiltration anesthesia: a prospective randomized double-blind cross-over study, J. Endod. 32 (2006) 296–298.
[6] D. Robertson, J. Nusstein, A. Reader, M. Beck, M. McCartney, The anesthetic efficacy of articaine in buccal infiltration of mandibular posterior teeth, J. Am. Dent. Assoc. 138 (2007) 1104–1112.
[7] J.-L. Lima-Júnior, E. Dias-Ribeiro, T.-N. de Araújo, J. Ferreira-Rocha, E.-S. Honfi-Júnior, C.-F. de Moraes Sarmento, F.-R.-G. Seabra, M. de Sousa, Evaluation of the buccal vestibule-palatal diffusion of 4% articaine hydrochloride in impacted maxillary third molar extractions, Med. Oral Patol. Oral Cir. Bucal 14 (2009) E129–E132.
[8] M.D. Kanaa, J.M. Whitworth, I.P. Corbett, J.G. Meechan, Articaine buccal infiltration enhances the effectiveness of lidocaine inferior alveolar nerve block, Int. Endod. J. 42 (2009) 238–246.
[9] W. Foster, M. Drum, A. Reader, M. Beck, Anesthetic efficacy of buccal and lingual infiltrations of lidocaine following an inferior alveolar nerve block in mandibular posterior teeth, Anesth. Prog. 54 (2007) 163–169.
[10] K.E. Schulze, P.R. Cohen, B.R. Nelson, Articaine: an effective adjunctive local anesthetic for painless surgery at the depth of the muscular fascia, Dermatol. Surg. 32 (2006) 407–410.
[11] M. Ozdemir, G. Ozdemir, B. Zencirci, H. Oksuz, Articaine versus lidocaine plus bupivacaine for peribulbar anaesthesia in cataract surgery, Br. J. Anaesth. 92 (2004) 231–234.
[12] G.K. Wang, J. Calderon, S.J. Jaw, S.Y. Wang, State-dependent block of Na +channels by articaine via the local anesthetic receptor, J. Membr. Biol. 229 (2009) 1–9.
[13] A. Sierra Rebolledo, E. Delgado Molina, L. Berini Aytés, C. Gay Escoda, Comparative study of the anesthetic efficacy of 4% articaine versus 2% lidocaine in inferior alveolar nerve block during surgical extraction of impacted lower third molars, Med. Oral Patol. Oral Cir. Bucal 12 (2007) E139–E144.
[14] P.T. Frangopol, D. Mihăilescu, Interactions of some local anesthetics and alcohols with membranes, Colloids Surf. B 22 (2001) 3–22.
[15] S. Chen, A.U. Gjerde, H. Holmsen, W. Nerdal, Importance of polyunsaturated acyl chains in chlorpromazine interaction with phosphatidylserines: a ^{13}C and ^{31}P solid-state NMR study, Biophys. Chem. 117 (2005) 101–109.
[16] C. Song, W. Nerdal, Olanzapine interaction with dipalmitoyl phosphatidylcholine (DPPC) and 1-palmitoyl-2-oleoyl phosphatidylserine (POPS) bilayer: A ^{13}C and ^{31}P solid-state NMR study, Biophys. Chem. 134 (2008) 47–55.
[17] C.J. Högberg, A.P. Lyubartsev, Effect of local anesthetic lidocaine on electrostatic properties of a lipid bilayer, Biophys. J. 94 (2008) 525–531.
[18] A.D. Mackerell Jr., Empirical force fields for biological macromolecules: overview and issues, J. Comput. Chem. 25 (2004) 1584–1604.
[19] S.-W. Chiu, M. Clark, V. Balaji, S. Subramaniam, H.L. Scott, E. Jakobsson, Incorporation of surface tension into molecular dynamics simulation of an interface: a fluid phase lipid bilayer membrane, Biophys. J. 69 (1995) 1230–1245.
[20] S.E. Feller, R.W. Pastor, On simulating lipid bilayers with an applied surface tension: periodic boundary conditions and undulations, Biophys. J. 71 (1996) 1350–1355.
[21] B. Jójárt, T.A. Martinek, Performance of the general amber force field in modeling aqueous POPC membrane bilayers, J. Comput. Chem. 28 (2007) 2051–2058.
[22] S.W.I. Siu, R. Vácha, P. Jungwirth, R.A. Böckmann, Biomolecular simulations of membranes: physical properties from different force fields, J. Chem. Phys. 128 (2008) 125103.
[23] R. Vácha, P. Jurkiewicz, M. Petrov, M.L. Berkowitz, R.A. Böckmann, J. Barucha-Kraszewska, M. Hof, P. Jungwirth, Mechanism of interaction of monovalent ions with phosphatidylcholine lipid membranes, J. Phys. Chem. B 114 (2010) 9504–9509.
[24] A.N. Gentilcore, N. Michaud-Agrawal, P.S. Crozier, M.J. Stevens, T.B. Woolf, Examining the origins of the hydration force between lipid bilayers using all-atom simulations, J. Membr. Biol. 235 (2010) 1–15.
[25] S. Mondal, C. Mukhopadhyay, Molecular insight of specific cholesterol interactions: a molecular dynamics simulation study, Chem. Phys. Lett. 439 (2007) 166–170.
[26] M.B. Tessier, M.L. DeMarco, A.B. Yongye, R.J. Woods, Extension of the GLYCAM06 biomolecular force field to lipids, lipid bilayers and glycolipids, Mol. Simul. 34 (2008) 349–363.
[27] M. Carrillo-Tripp, S.E. Feller, Evidence for a mechanism by which ω-3 polyunsaturated lipids may affect membrane protein function, Biochemistry 44 (2005) 10164–10169.
[28] S.E. Feller, Acyl chain conformations in phospholipid bilayers: a comparative study of docosahexaenoic acid and saturated fatty acids, Chem. Phys. Lipids 153 (2008) 76–80.
[29] J. Hénin, W. Shinoda, M.L. Klein, United-atom acyl chains for CHARMM phospholipids, J. Phys. Chem. B 112 (2008) 7008–7015.
[30] J. Lee, W. Im, Role of hydrogen bonding and helix–lipid interactions in transmembrane helix association, J. Am. Chem. Soc. 130 (2008) 6456–6462.

[31] P. Prakash, R. Sankararamakrishnan, Force field dependence of phospholipid headgroup and acyl chain properties: comparative molecular dynamics simulations of DMPC bilayers, J. Comput. Chem. 31 (2010) 266–277.

[32] C.-J. Högberg, A.M. Nikitin, A.P. Lyubartsev, Modification of the CHARMM force field for DMPC lipid bilayer, J. Comput. Chem. 29 (2008) 2359–2369.

[33] J.B. Klauda, R.M. Venable, J.A. Freites, J.W. O'Connor, D.J. Tobias, C. Mondragon-Ramirez, I. Vorobyov, A.D. MacKerell Jr., R.W. Pastor, Update of the CHARMM all-atom additive force field for lipids: validation on six lipid types, J. Phys. Chem. B 114 (2010) 7830–7843.

[34] J. Taylor, N.E. Whiteford, G. Bradley, G.W. Watson, Validation of all-atom phosphatidylcholine lipid force fields in the tensionless NPT ensemble, Biochim. Biophys. Acta Biomembr. 1788 (2009) 638–649.

[35] D. Poger, W.F. Van Gunsteren, A.E. Mark, A new force field for simulating phosphatidylcholine bilayers, J. Comput. Chem. 31 (2010) 1117–1125.

[36] D.A. Case, T.E. Cheatham III, T. Darden, H. Gohlke, R. Luo, K.M. Merz Jr., A. Onufriev, C. Simmerling, B. Wang, R.J. Woods, The Amber biomolecular simulation programs, J. Comput. Chem. 26 (2005) 1668–1688.

[37] D.A. Case, T.A. Darden, I. Cheatham, T. E., C.L. Simmerling, J. Wang, R.E. Duke, R. Luo, K.M. Merz, D.A. Pearlman, M. Crowley, R.C. Walker, W. Zhang, B. Wang, S. Hayik, A. Roitberg, G. Seabra, K.F. Wong, F. Paesani, X. Wu, S. Brozell, V. Tsui, H. Gohlke, L. Yang, C. Tan, J. Mongan, V. Hornak, G. Cui, P. Beroza, D.H. Mathews, C. Schafmeister, W.S. Ross, P.A. Kollman, AMBER 9, University of California, San Francisco, 2006.

[38] J. Wang, R.M. Wolf, J.W. Caldwell, P.A. Kollman, D.A. Case, Development and testing of a general amber force field, J. Comput. Chem. 25 (2004) 1157–1174.

[39] L. Rosso, I.R. Gould, Structure and dynamics of phospholipid bilayers using recently developed general all-atom force fields, J. Comput. Chem. 29 (2008) 24–37.

[40] R. Maget-Dana, The monolayer technique: a potent tool for studying the interfacial properties of antimicrobial and membrane-lytic peptides and their interactions with lipid membranes, Biochim. Biophys. Acta Biomembr. 1462 (1999) 109–140.

[41] W.R. Glomm, S. Volden, Ø. Halskau Jr., M.-H.G. Ese, Same system-different results: the importance of protein-introduction protocols in Langmuir-monolayer studies of lipid–protein interactions, Anal. Chem. 81 (2009) 3042–3050.

[42] M.J. Frisch, G.W. Trucks, H.B. Schlegel, G.E. Scuseria, M.A. Robb, J.R. Cheeseman, J.A. Montgomery Jr., T. Vreven, K.N. Kudin, J.C. Burant, J.M. Millam, S.S. Iyengar, J. Tomasi, V. Barone, B. Mennucci, M. Cossi, G. Scalmani, N. Rega, G.A. Petersson, H. Nakatsuji, M. Hada, M. Ehara, K. Toyota, R. Fukuda, J. Hasegawa, M. Ishida, T. Nakajima, Y. Honda, O. Kitao, H. Nakai, M. Klene, X. Li, J.E. Knox, H.P. Hratchian, J.B. Cross, C. Adamo, J. Jaramillo, R. Gomperts, R.E. Stratmann, O. Yazyev, A.J. Austin, R. Cammi, C. Pomelli, J.W. Ochterski, P.Y. Ayala, K. Morokuma, G.A. Voth, P. Salvador, J.J. Dannenberg, V.G. Zakrzewski, S. Dapprich, A.D. Daniels, S.M. C., O. Farkas, D.K. Malick, A.D. Rabuck, K. Raghavachari, J.B. Foresman, J.V. Ortiz, Q. Cui, A.G. Baboul, S. Clifford, J. Cioslowski, B.B. Stefanov, G. Liu, A. Liashenko, P. Piskorz, I. Komaromi, R.L. Martin, D.J. Fox, T. Keith, M.A. Al-Laham, C.Y. Peng, A. Nanayakkara, M. Challacombe, P.M.W. Gill, B. Johnson, W. Chen, M.W. Wong, C. Gonzalez, J.A. Pople, Gaussian 03, Gaussian, Inc., Pittsburgh PA, 2003.

[43] C.I. Bayly, P. Cieplak, W.D. Cornell, P.A. Kollman, A well-behaved electrostatic potential based method using charge restraints for deriving atomic charges: the RESP model, J. Phys. Chem. 97 (1993) 10269–10280.

[44] J. Wang, W. Wang, P.A. Kollman, D.A. Case, Automatic atom type and bond type perception in molecular mechanical calculations, J. Mol. Graph. Model. 25 (2006) 247–260.

[45] http://www.apmaths.uwo.ca/~mkarttu/downloads.shtml.

[46] W.L. Jorgensen, J. Chandrasekhar, J.D. Madura, R.W. Impey, M.L. Klein, Comparison of simple potential functions for simulating liquid water, J. Chem. Phys. 79 (1983) 926–935.

[47] T. Darden, D. York, L. Pedersen, Particle mesh Ewald: an $N\log(N)$ method for Ewald sums in large systems, J. Chem. Phys. 98 (1993) 10089–10092.

[48] U. Essmann, L. Perera, M.L. Berkowitz, T. Darden, H. Lee, L.G. Pedersen, A smooth particle mesh Ewald method, J. Chem. Phys. 103 (1995) 8577–8593.

[49] J.-P. Ryckaert, G. Ciccotti, H.J.C. Berendsen, Numerical integration of the cartesian equations of motion of a system with constraints: molecular dynamics of n-alkanes, J. Comput. Phys. 23 (1977) 327–341.

[50] M.Ø. Jensen, O.G. Mouritsen, G.H. Peters, Simulations of a membrane-anchored peptide: structure, dynamics, and influence on bilayer properties, Biophys. J. 86 (2004) 3556–3575.

[51] É.T. Prates, P.C.T. Souza, M. Pickholz, M.S. Skaf, Charmm-based parameterization of neutral articaine—a widely used local anesthetic, Int. J. Quantum Chem. (in press), Epub ahead of print.

[52] B.R. Brooks, C.L. Brooks III, A.D. Mackerell Jr., L. Nilsson, R.J. Petrella, B. Roux, Y. Won, G. Archontis, C. Bartels, S. Boresch, A. Caflisch, L. Caves, Q. Cui, A.R. Dinner, M. Feig, S. Fischer, J. Gao, M. Hodoscek, W. Im, K. Kuczera, T. Lazaridis, J. Ma, V. Ovchinnikov, E. Paci, R.W. Pastor, C.B. Post, J.Z. Pu, M. Schaefer, B. Tidor, R.M. Venable, H.L. Woodcock, X. Wu, W. Yang, D.M. York, M. Karplus, CHARMM: the biomolecular simulation program, J. Comput. Chem. 30 (2009) 1545–1614.

[53] J.C. Phillips, R. Braun, W. Wang, J. Gumbart, E. Tajkhorshid, E. Villa, C. Chipot, R.D. Skeel, L. Kalé, K. Schulten, Scalable molecular dynamics with NAMD, J. Comput. Chem. 26 (2005) 1781–1802.

[54] R.J. Loncharich, B.R. Brooks, R.W. Pastor, Langevin dynamics of peptides: the frictional dependence of isomerization rates of N-acetylalanyl-N'-methylamide, Biopolymers 32 (1992) 523–535.

[55] H.J.C. Berendsen, J.P.M. Postma, W.F. van Gunsteren, A. DiNola, J.R. Haak, Molecular dynamics with coupling to an external bath, J. Chem. Phys. 81 (1984) 3684–3690.

[56] http://www.avantilipids.com/index.php?option=com_content&view=article&id=1700&Itemid=419.

[57] W. Humphrey, A. Dalke, K. Schulten, VMD: visual molecular dynamics, J. Mol. Graph. 14 (1996) 33–38.

[58] B.K. Shoichet, I.D. Kuntz, D.L. Bodian, Molecular docking using shape descriptors, J. Comput. Chem. 13 (1992) 380–397.

[59] E.C. Meng, B.K. Shoichet, I.D. Kuntz, Automated docking with grid-based energy evaluation, J. Comput. Chem. 13 (1992) 505–524.

[60] D. van der Spoel, E. Lindahl, B. Hess, G. Groenhof, A.E. Mark, H.J.C. Berendsen, GROMACS: fast, flexible, and free, J. Comput. Chem. 26 (2005) 1701–1718.

[61] D. Marsh, Lateral pressure in membranes, Biochim. Biophys. Acta 1286 (1996) 183–223.

[62] B. Perly, I.C.P. Smith, H.C. Jarrell, Effects of the replacement of a double bond by a cyclopropane ring in phosphatidylethanolamines: a ^{2}H NMR study of phase transitions and molecular organization, Biochemistry 24 (1985) 1055–1063.

[63] J. Seelig, N. Waespe-Šarčević, Molecular order in cis and trans unsaturated phospholipid bilayers, Biochemistry 17 (1978) 3310–3315.

[64] J.M. Smaby, M.M. Momsen, H.L. Brockman, R.E. Brown, Phosphatidylcholine acyl unsaturation modulates the decrease in interfacial elasticity induced by cholesterol, Biophys. J. 73 (1997) 1492–1505.

[65] P.A. Hyslop, B. Morel, R.D. Sauerheber, Organization and interaction of cholesterol and phosphatidylcholine in model bilayer membranes, Biochemistry 29 (1990) 1025–1038.

[66] N. Kučerka, S. Tristram-Nagle, J.F. Nagle, Structure of fully hydrated fluid phase lipid bilayers with monounsaturated chains, J. Membr. Biol. 208 (2005) 193–202.

[67] G. Pabst, M. Rappolt, H. Amenitsch, P. Laggner, Structural information from multilamellar liposomes at full hydration: full q-range fitting with high quality x-ray data, Phys. Rev. E: Stat. Phys. Plasmas Fluids Relat. Interdisciplin. Top. 62 (2000) 4000–4009.

[68] A. Seelig, J. Seelig, Effect of a single cis double bond on the structure of a phospholipid bilayer, Biochemistry 16 (1977) 45–50.

[69] E. Strandberg, J.A. Killian, Snorkeling of lysine side chains in transmembrane helices: how easy can it get? FEBS Lett. 544 (2003) 69–73.

[70] C. Song, H. Lygre, W. Nerdal, Articaine interaction with DSPC bilayer: A ^{13}C and ^{31}P solid-state NMR study, Eur. J. Pharm. Sci. 33 (2008) 399–408.

[71] H. Lygre, G. Moe, W. Nerdal, H. Holmsen, Interaction of articaine hydrochloride with prokaryotic membrane lipids, Acta Odontol. Scand. 67 (2009) 1–7.

[72] C.J. Högberg, A. Maliniak, A.P. Lyubartsev, Dynamical and structural properties of charged and uncharged lidocaine in a lipid bilayer, Biophys. Chem. 125 (2007) 416–424.

[73] B. Kuhn, P. Mohr, M. Stahl, Intramolecular hydrogen bonding in medicinal chemistry, J. Med. Chem. 53 (2010) 2601–2611.

[74] C. Hansch, A. Leo, D. Hoekman, Exploring QSAR. Hydrophobic, electronic, and steric constants, American Chemical Society, Washington DC, 1995.

[75] J.E. John, Natural products-based drugs and membrane permeability, a hypothesis, Chem. Biol. Drug Des. 73 (2009) 367–368.

[76] P.R. Overman, Articaine: a new alternative in dental hygiene pain control, J. Dent. Hyg. 81 (2007) 66.